

Stabilization Method for DC-bus Oscillation in Dynamic Wireless Power Transfer Systems

Yuki Ochiai, Keisuke Kusaka

Dept. of Electrical, Electronics, and Information Engineering

Nagaoka University of Technology

Nagaoka, Japan

Email: s235022@stn.nagaokaut.ac.jp, kusaka@vos.nagaokaut.ac.jp

Abstract— Dynamic wireless power transfer systems will have a DC bus, which supplies power to inverters with transmission coils intermittently placed over long distances on the road surface. As the length of the DC bus increases, the wiring inductance also increases. This effect affects inverters that are located far from the power source of the DC bus, requiring them to connect through this increased wiring inductance. When the inverter performs current control on the output side, it may cause negative impedance, resulting in the DC-bus voltage oscillation. This paper proposes a control method to prevent instability of the DC bus voltage by utilizing positive feed-forward (PFF) control. The experimental results with the small-scale prototype show that the proposed control effectively prevents instability.

Keywords— DC power supply, Feed-forward control, Dynamic wireless power transfer, Magnetic resonance coupling, Electric vehicle

I. INTRODUCTION

In recent years, the transition from gasoline and diesel vehicles to electric vehicles (EVs) has been actively promoted to reduce greenhouse gas emissions. However, the current adoption rate of EVs remains low. This is primarily due to several challenges, such as the high cost of EVs caused by expensive batteries, the long charging times, and the limited driving range. To address these issues, wireless power transfer (WPT) for EVs during motion has been extensively studied [1]-[3]. Implementing in-motion WPT technology can extend the driving range even with smaller onboard batteries. Consequently, the smaller battery capacity reduces the overall cost of EVs. Furthermore, the ability to charge vehicles while driving eliminates the need to stop to recharge. These advantages suggest that the practical adoption of in-motion WPT could significantly accelerate the widespread use of EVs.

A system configuration for a dynamic WPT has been proposed, as shown in Fig. 1 [4]. In this configuration, multiple primary coils are embedded intermittently along the roadway. Each transmission coil is connected to an inverter, which supplies power to the coil. The inverters are connected to a DC bus that runs along the roadway. The length of the DC bus may be long since the WPT system is expected to be applied to highways. As the DC bus length increases, the wiring inductance also becomes significant. Consequently, inverters far from the AC-DC converter that supplies power to the DC bus are connected via non-negligible wiring inductance. In such a system, if output power is controlled on the inverter side, negative resistance caused by the inverter's control may lead to oscillation in the DC-link capacitor voltage [7].

This paper aims to clarify the instability conditions of the WPT system. First, a simplified model is constructed to represent the system under conditions where the wiring inductance is sufficiently large and instability occurs. Then, a control method is proposed to prevent instability by applying a positive feedforward (PFF) control strategy [8] to the simplified model.

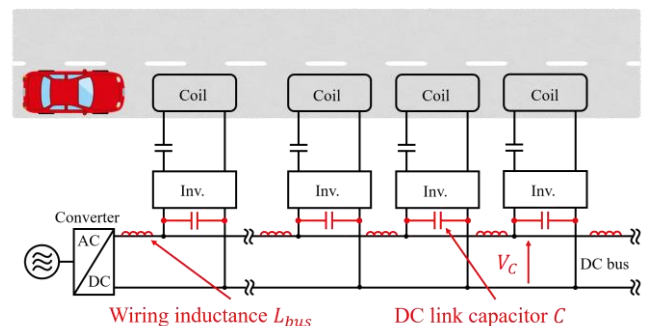


Fig. 1. System structure of dynamic charging for electric vehicles.

II. DC BUS VOLTAGE INSTABILITY CONDITIONS

Using a simplified model, this chapter derives the instability conditions for inverters connected via the DC bus in the in-motion WPT system. In the in-motion wireless power transfer (WPT) system shown in Fig. 1, power is supplied to each inverter through the DC bus from an AC-DC converter that serves as the DC power source. When each inverter performs output power control, negative resistance is introduced by the feedback control of the inverter. The negative resistance, combined with the wiring inductance of the DC bus, may cause an oscillation in the DC-link voltage. The next paragraph will explain the instability conditions for inverters connected via the DC bus using a simplified model.

The instability conditions are developed from the simplified model of the dynamic WPT. Fig. 2 illustrates the simplified system used to derive the instability conditions of the WPT system. In this system, V_g represents the voltage source supplying power to the DC bus, while L_{bus} and R_{bus} denote the wiring inductance and resistance of the DC bus, respectively. The "Constant power load" in Fig. 2 represents a power transmission unit far from the DC bus voltage source. This unit behaves as a constant power load (CPL) due to feedback control. Fig. 3 shows the current-voltage (I-V) characteristics of the CPL. The slope of the tangent at an operating point, dv_{in} / di_b , is equivalent to a resistance-like parameter and is denoted as r' . At the operating point v_{in} , r' is expressed as follows:

$$r' = \frac{dv_{in}}{di_b} = -\frac{v_{in}^2}{P} \quad (1)$$

In this paragraph, the stability conditions are derived. The negative resistance r' may cancel the resistive component R_{bus} of the wiring under certain conditions. This is known to cause oscillations between the wiring inductor L_{bus} and the input capacitor C_{s1} .

Assume that in Fig. 2, the supply voltage V_g momentarily changes by Δv_g to $V_g + \Delta v_g$. It causes the change in the current flowing through the inductor and the load voltage. The current flowing in the inductor changes by Δi_{in} from I_{in} to $I_{in} + \Delta i_{in}$. Also, the load voltage changes by Δv_{in} from V_{in} to $V_{in} + \Delta v_{in}$. The following equation is developed from these changes.

$$\begin{bmatrix} \Delta \dot{v}_{in} \\ \Delta \dot{i}_{in} \end{bmatrix} = \begin{bmatrix} \frac{P}{C_{s1}V_{in}^2} & \frac{1}{C_{s1}} \\ \frac{1}{L_{bus}} & -\frac{R_{bus}}{L_{bus}} \end{bmatrix} \begin{bmatrix} \Delta v_{in} \\ \Delta i_{in} \end{bmatrix} + \begin{bmatrix} 0 \\ \frac{1}{L_{bus}} \end{bmatrix} \Delta v_g \quad (2)$$

$$A = \begin{bmatrix} \frac{P}{C_{s1}V_{in}^2} & \frac{1}{C_{s1}} \\ \frac{1}{L_{bus}} & -\frac{R_{bus}}{L_{bus}} \end{bmatrix} \quad (3)$$

The characteristic equation $\Delta(s)$ of this system is expressed as Eq. (4), where I is the identity matrix. Applying the Routh-Hurwitz stability criterion to Eq. (4), the stability conditions can be derived as follows:

$$\Delta(s) = \det[sI - A] \quad (4)$$

$$-\frac{P}{C_{s1}V_{in}^2} + \frac{R_{bus}}{L_{bus}} > 0 \quad (6)$$

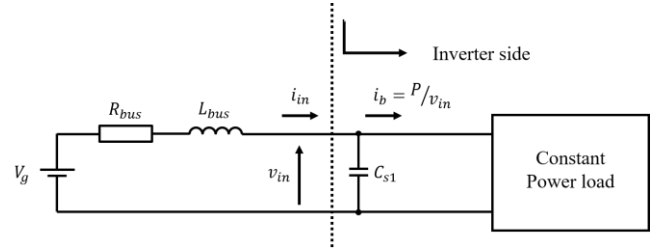


Fig. 2. A simple system concerning instability caused by constant power loads.

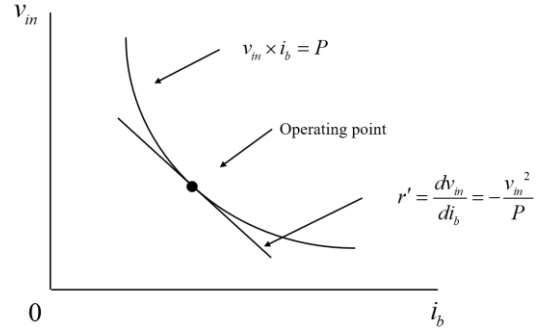


Fig. 3. Negative impedance behavior of constant power load.

$$\Delta(s) = \det \begin{bmatrix} s - \frac{P}{C_{s1}V_{in}^2} & \frac{1}{C_{s1}} \\ \frac{1}{L_{bus}} & s + \frac{R_{bus}}{L_{bus}} \end{bmatrix} = s^2 + \left(-\frac{P}{C_{s1}V_{in}^2} + \frac{R_{bus}}{L_{bus}} \right) s - \frac{PR_{bus}}{C_{s1}L_{bus}V_{in}^2} + \frac{1}{C_{s1}L_{bus}} \quad (5)$$

$$\alpha = 2\cos^{-1}\left(\frac{\pi}{2\sqrt{2}}\frac{E_{ie}}{V_g}\right) \quad (9)$$

$$-\frac{PR_{bus}}{C_{s1}L_{bus}V_{in}^2} + \frac{1}{C_{s1}L_{bus}} > 0 \quad (7)$$

Simplifying Eq. (7) results in:

$$-\frac{PR_{bus}}{V_{in}^2} + 1 > 0 \quad (8)$$

Thus, an oscillation in the DC bus voltage will occur if both Eqs. (6) and (8) are not satisfied.

III. PROPOSED CONTROL METHOD

A. System Overview

Fig. 4 shows the circuit diagram of the wireless power transfer (WPT) system, including the DC bus. In this circuit, wiring inductance and resistance components are inserted between the DC bus power source and the inverter to simulate a power transmission unit far from the DC power source. Fig. 5 presents the control block diagram of the inverter. In this control scheme, since the switching frequency is high, a constant current is supplied to the primary coil by controlling the envelope i_{ie} , which connects the peak values of the primary sinusoidal current.

As shown in Fig. 6, a peak detection circuit is used to detect the current envelope i_{ie} . The voltage V_{il} represents the signal from the current sensor, and V_{ie} is the output signal of the peak detection circuit. This circuit utilizes the forward characteristics of the diode; when V_{il} exceeds the voltage of capacitor C_p , the capacitor is charged. Then, the circuit outputs the peak value of V_{il} at all times. Using this circuit, the envelope is detected from the primary current of the WPT system, and the phase shift α of the inverter output is adjusted via feedback control. Specifically, Eq. (9) in Fig. 5 describes the conversion of the PI controller's output into the phase shift α .

However, this feedback control lets the inverter behave as a negative resistance, leading to oscillations in the DC bus voltage. Positive feed-forward (PFF) control is introduced into the control block to address this issue. PFF control detects the fluctuation component of the DC-link voltage V_c using a high-pass filter. The fluctuation component is then multiplied by a gain K_F and added to the error in the feedback loop to mitigate instability.

B. Derivation of plant models and design of PI controllers

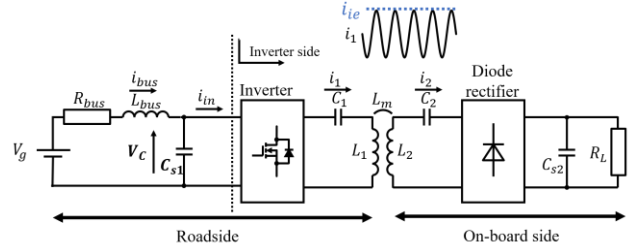


Fig. 4. Circuit configuration emulating a DC bus and unit.

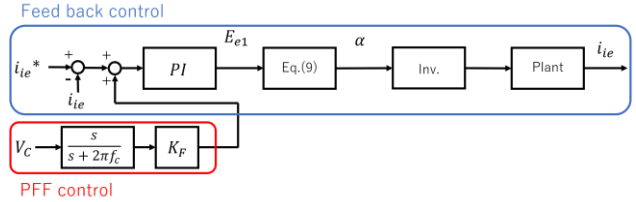


Fig. 5. Control block diagram.

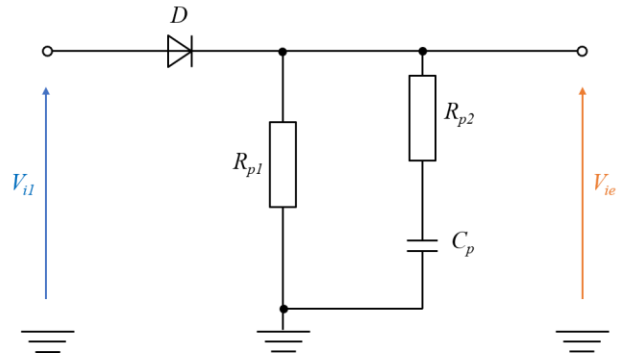


Fig. 6. Peak detection circuit.

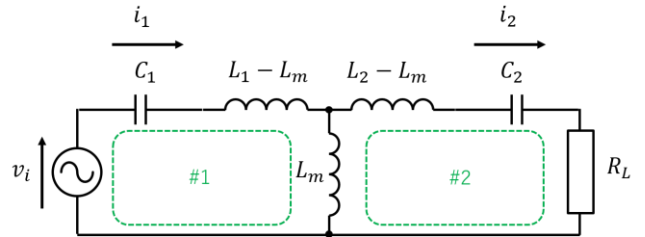


Fig. 7. T-type equivalent circuit.

To design the control system, the transfer function of the plant for control of the envelope of the primary current in the series-series (S/S) resonant circuit is derived in this section. Fig. 7 shows the equivalent T-type circuit of the S/S resonant circuit, where the internal resistances of the primary and secondary coils are neglected for simplicity.

Eq. (11) and (12) are obtained from Fig. 7, defining two current loops I_1 and I_2 . Here, the following approximate equation is obtained. In equation (12), $1 / \omega_o$ appears each time a partial integral is performed. This time, we simplify the equation by ignoring the third terms because the third term is proportional to the inverse cube of the angular frequency ω .

$$v_1 = \frac{1}{C_1} \int i_1(t) dt + (L_1 - L_M) \frac{di_1(t)}{dt} + L_M \left(\frac{di_1(t)}{dt} - \frac{di_2(t)}{dt} \right) \quad (10)$$

$$L_M \left(\frac{di_1(t)}{dt} - \frac{di_2(t)}{dt} \right) = (L_2 - L_M) \frac{di_2(t)}{dt} + \frac{1}{C_2} \int i_2(t) dt + R_L i_2(t) \quad (11)$$

$$\begin{aligned} \frac{1}{C_1} \int i_1(t) dt &= \frac{1}{C_1} \int I_1 \sin(\omega_o t) dt \\ &= \frac{-1}{\omega_o C_1} \left(I_1 \cos(\omega_o t) - \int \frac{dI_1(t)}{dt} \cos(\omega_o t) dt \right) \\ &= \frac{-1}{\omega_o C_1} \left\{ I_1 \cos(\omega_o t) - \frac{1}{\omega_o} \left(\frac{dI_1(t)}{dt} \sin(\omega_o t) - \int \frac{d^2 I_1(t)}{dt^2} \sin(\omega_o t) dt \right) \right\} \\ &= \frac{-1}{\omega_o C_1} \left[I_1 \cos(\omega_o t) - \frac{1}{\omega_o} \left\{ \frac{dI_1(t)}{dt} \sin(\omega_o t) + \frac{1}{\omega_o} \left(\frac{d^2 I_1(t)}{dt^2} \cos(\omega_o t) - \int \frac{d^3 I_1(t)}{dt^3} \cos(\omega_o t) dt \right) \right\} \right] \\ &= \frac{-1}{\omega_o C_1} I_1 \cos(\omega_o t) + \frac{1}{\omega_o^2 C_1} \frac{dI_1(t)}{dt} \sin(\omega_o t) - \frac{1}{\omega_o^3 C_1} \left(\frac{d^2 I_1(t)}{dt^2} \cos(\omega_o t) - \int \frac{d^3 I_1(t)}{dt^3} \cos(\omega_o t) dt \right) \\ &\approx \frac{-1}{\omega_o C_1} I_1 \cos(\omega_o t) + \frac{1}{\omega_o^2 C_1} \frac{dI_1(t)}{dt} \sin(\omega_o t) \\ R_L V_1 + 2L_2 \frac{dV_1(t)}{dt} &= 4L_1 L_2 \frac{d^2 I_1(t)}{dt^2} + 2L_1 R_L \frac{dI_1(t)}{dt} + (\omega_o L_M)^2 I_1(t) \end{aligned} \quad (12)$$

$$\begin{aligned} L_M \frac{di_2(t)}{dt} &= L_M \left(\frac{di_2(t)}{dt} \cos(\omega_o t) - \omega_o I_2(t) \sin(\omega_o t) \right) \\ &\approx \omega_o L_M I_2 \sin(\omega_o t) \end{aligned} \quad (13)$$

$$V_1(t) = 2L_1 \frac{dI_1(t)}{dt} + \omega_o L_M I_2(t) \quad (14)$$

$$\omega_o L_M I_1(t) = 2L_2 \frac{dI_2(t)}{dt} + R_L I_2(t) \quad (15)$$

By eliminating $I_2(t)$ from Eqs. (14) and (15), the following equation is Eq. (16).

Taking the Laplace transform of Eq. (16), the envelope model from V_1 to I_1 is expressed as Eq. (17):

$$G(s) = \frac{\frac{1}{2L_1} s + \frac{R_L}{4L_1 L_2}}{s^2 + \frac{R_L}{2L_2} s + \frac{(\omega L_M)^2}{4L_1 L_2}} \quad (17)$$

Here,

$$L_M = k \sqrt{L_1 L_2} \quad (18)$$

allowing for the following rearrangement:

$$P(s) = \frac{\frac{1}{2L_1} s + \frac{R_L}{4L_1 L_2}}{s^2 + \frac{R_L}{2L_2} s + \frac{\omega_o^2 k^2}{4}} \quad (19)$$

Assuming $L_1 = L_2 = L$, the equation can be further simplified to:

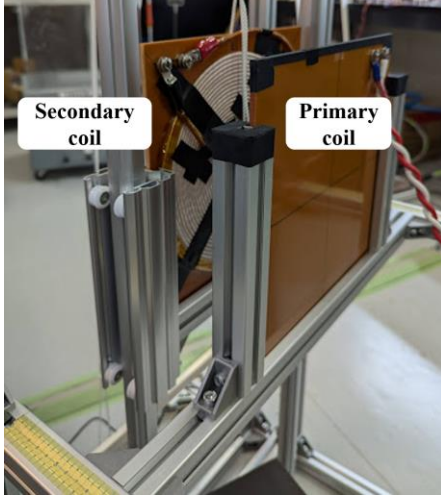
$$P(s) = \frac{2Ls + R_L}{4L^2 s^2 + 2LR_L s + L^2 \omega_o^2 k^2} \quad (20)$$

Eq. (20) represents the plant's transfer function used in this study.

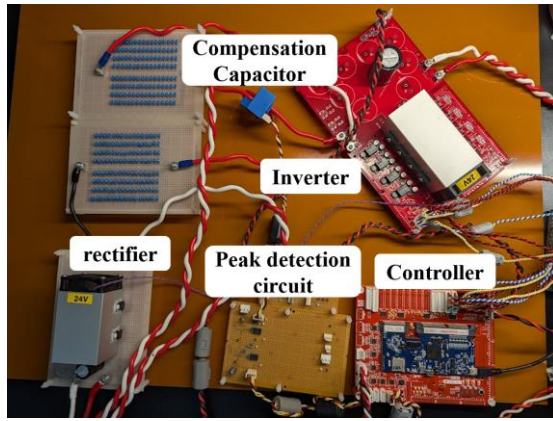
Using this plant's transfer function, the proportional gain K_p and integral gain K_i were determined via pole placement. The resulting values are $K_p = 0.50$ and $K_i = 5500$.

C. PFF controller settings

This section describes the gain settings of the PFF controller. The gain K_F of the PFF controller in Fig. 5 is determined from the disturbance transfer function. The disturbance transfer function from the detected DC link voltage V_c to the plant output I_{ie} depends on the gain K_F of the PFF controller. To suppress oscillations in the DC bus voltage, it is desirable for the disturbance transfer function to remain below 0dB. To satisfy this condition, K_F must be set to a value less than 1. If K_F is negative, the phase is inverted, which amplifies the oscillations of V_c . Therefore, K_F must satisfy $0 < K_F < 1$.



(a) Coils



(b) Circuit

Fig. 8. Experimental setup.

Table 1. Parameters of scaled-model.

Parameter	Symbol	Value
DC bus voltage	V_s	70.0 V
Resonant frequency	f_o	85.0 kHz
Load resistance	R_L	6.67 Ω
Transmitting coil	L_1, L_2	63.2 μH
ESR	R_1, R_2	0.320 Ω
Compensation Capacitor	C_1, C_2	55.4 nF
Wire resistance	R_{bus}	0.1 Ω
Wire inductor	L_{bus}	5.5 mH
Primary DC link capacitor	C_{s1}	470 μF
Secondary DC link capacitor	C_{s2}	120 μF

which may limit the power transmission capacity of the DWPT system. Additionally, since the output signal of the PFF controller is added to the input of the PI controller, a larger output signal from the PFF controller increases the error relative to the current reference value.

To address these issues, K_F should be set to a small value within the range $0 < K_F < 1$, ensuring that the maximum V_c during instability is kept below a desired threshold.

IV. EXPERIMENTAL RESULTS

The stability limits and the effects of PFF control were experimentally verified using a mini-model. Fig. 8 shows the appearance of the experimental setup. The mini-model circuit configuration is depicted in Fig. 9, and the circuit parameters are listed in Table 1. The resonance circuit and load parameters were designed for maximum efficiency based on the required maximum power and the DC bus power supply voltage [12].

First, the current reference was step-changed between stable and unstable conditions to confirm the DC bus oscillation conditions in this system. Fig. 9 shows the DC bus voltage when the reference value was step-changed from 0.42 to 0.50 p.u. According to the stability conditions derived from Eq. (6) and Eq. (8), the system exceeded the stability limit as the primary current increased from 0.42 to 0.50 p.u., confirming the stability conditions through experimental validation.

Fig. 10 shows the DC link voltage when PFF control was applied during operation. In this experiment, PFF control was applied to stabilize the system after the DC link voltage began oscillating, with the reference value set at 0.67 p.u. From Fig. 10, it was confirmed that applying PFF control successfully avoided instability. The oscillation frequency of the DC link voltage was approximately 98 Hz, which matched the resonant frequency of the DC bus wiring inductance and the DC link capacitor.

Finally, Fig. 11 illustrates the relationship between K_F , the maximum DC link voltage V_{c_max} , and the rise time T_r . As K_F increases, V_{c_max} decreases, but the rise time becomes longer, reducing the chargeable power. Therefore, K_F should be set to a small value within the range that suppresses V_c to an acceptable maximum DC link voltage while ensuring adequate rise time.

V. CONCLUSIONS

This study introduced a control method that integrates positive feed-forward (PFF) control with current envelope control to prevent oscillations in the DC link voltage of a

wireless power transfer system with an extended DC bus. Experimental validation demonstrated that the application of PFF control effectively mitigates instability. Furthermore, it was found that increasing the PFF control gain led to a longer rise time and a decrease in the maximum DC link voltage.

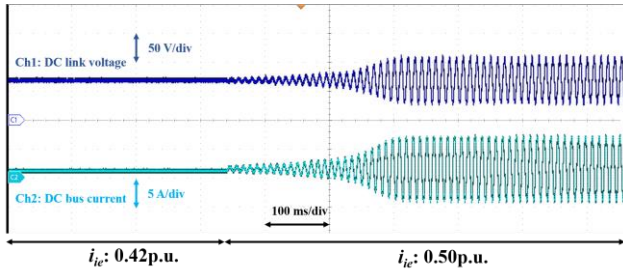


Fig. 9. Oscillation waveform at stability limit by measurement.

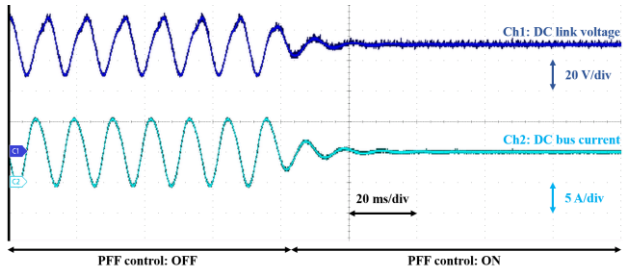


Fig. 10. Oscillation comparison with PFF control.

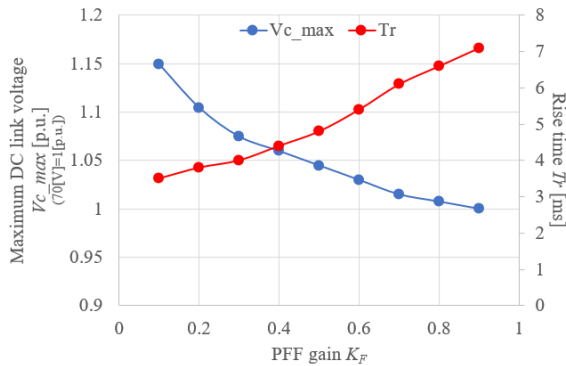


Fig. 11. Relationship between KF and V_{c_max} , T_r .

REFERENCES

- [1] Zhang, Zhen, et al. "Wireless power transfer—An overview." *IEEE transactions on industrial electronics* 66.2 (2018): 1044-1058.
- [2] Mahesh, Aganti, Bharatiraja Chokkalingam, and Lucian Mihet-Popa. "Inductive wireless power transfer charging for electric vehicles—a review." *IEEE access* 9 (2021): 137667-137713.
- [3] Feng, Hao, et al. "An LCC-compensated resonant converter optimized for robust reaction to large coupling variation in dynamic wireless power transfer." *IEEE Transactions on Industrial Electronics* 63.10 (2016): 6591-6601.

- [4] Daita Kobayashi, Takehiro Imura, Yoichi Hori, "Real-time Maximum Efficiency Control in Dynamic Wireless Power Transfer System" *IEEE Transaction on Industry Applications* Vol.136 No.6 pp.425-432 (2016).
- [5] Zhang, Xin, et al. "Adaptive active capacitor converter for improving stability of cascaded DC power supply system." *IEEE Transactions on Power Electronics* 28.4 (2012): 1807-1816.
- [6] Zhang, Xin, Qing-Chang Zhong, and Wen-Long Ming. "Stabilization of cascaded DC/DC converters via adaptive series-virtual-impedance control of the load converter." *IEEE Transactions on Power Electronics* 31.9 (2016): 6057-6063.
- [7] K. Miura, H. Watanabe, J. -i. Itoh, T. Kiribuchi and H. Tokusaki, "Damping Controller Integrated into Output Current Control Loop and Design for Multiple Servo Drive Systems Connected to Common DC-Bus Line," 2023 IEEE Applied Power Electronics Conference and Exposition (APEC), Orlando, FL, USA, 2023, pp. 2367-2374, doi: 10.1109/APEC43580.2023.10131476.
- [8] Jeung, Yoon-Cheul, et al. "Design of passivity-based damping controller for suppressing power oscillations in DC microgrids." *IEEE Transactions on Power Electronics* 36.4 (2020): 4016-4028.
- [9] S. Chen and T. Czaszejko, "Partial discharge test circuit as a spark-gap transmitter," in *IEEE Electrical Insulation Magazine*, vol. 27, no. 3, pp. 36-44, May-June 2011.
- [10] Daisuke GUNJI, Takehiro IMURA, Hiroshi FUJIMOTO. "Secondary Voltage Envelope Model and Application to Control System Design on Wireless Power Transfer using Magnetic Resonance Coupling." *THE INSTITUTE OF ELECTRONICS, INFORMATION AND COMMUNICATION ENGINEERS* (2014): 45-50.
- [11] T. Hamada, T. Fujita and H. Fujimoto, "Fast Start-Up Control of Both-Side Current Without Overshoot Focusing on Rectification Timing for Dynamic Wireless Power Transfer Systems," in *IEEE Journal of Emerging and Selected Topics in Industrial Electronics*, vol. 5, no. 3, pp. 1039-1047, July 2024, doi: 10.1109/JESTIE.2023.3288476.
- [12] Bosshard, Roman, et al. "Modeling and η - α Pareto Optimization of Inductive Power Transfer Coils for Electric Vehicles." *IEEE Journal of Emerging and Selected Topics in Power Electronics* 3.1 (2014):